# POLITECNICO DI TORINO
## Repository ISTITUZIONALE

Autonomous Raman Amplifiers using Standard Integrated Network Equipment

(Article begins on next page)

08 November 2022

# Autonomous Raman Amplifiers using Standard Integrated Network Equipment

Giacomo Borraccini$^{(1)}$*, Stefano Staullu$^{(2)}$, Stefano Piciaccia$^{(3)}$, Alberto Tanzi$^{(3)}$,
Antonino Nespola$^{(2)}$, Gabriele Galimberti$^{(3)}$, and Vittorio Curri$^{(1)}$

$^{(1)}$ Politecnico di Torino, Turin, Italy, $^{(2)}$ LINKS Foundation, Turin, Italy, $^{(3)}$ Cisco Photonics, Vimercate, Italy

*giacomo.borraccini@polito.it*

*Abstract*—**Practical needs related to infrastructure management are driving optical network operators to include Raman amplification in order to improve the performance of long fiber spans. Compared to standard erbium-doped fiber amplifier (EDFA) management, Raman amplifiers require a greater degree of control and monitoring due to their distributed nature. Inevitably, this update leads to a key consideration; the introduction of additional telemetry devices with respect to standard EDFA photodiodes, resulting in an increase in required investments. In this work, we present an embedded controller architecture in combination with an ad-hoc probing procedure to manage Raman amplification within disaggregated optical networks, using only standard integrated equipment, allowing an efficient implementation without the introduction of optical channel monitors (OCMs). This proposal is validated using a fully representative experimental campaign, testing both the probing procedure on a single fiber span and the operation of a Raman amplifier using the extracted information.**

*Index Terms*—**Raman amplification, disaggregated optical networks, standard integrated equipment.**

## I. INTRODUCTION

**N**OWADAYS, Raman amplification is consistently used in the field of optical communications to realize highly-capacitive, long-haul transmission systems [1] thanks to its benefits in terms of noise reduction and efficiency on dense wavelength division multiplexing (DWDM) propagation [2]–[4]. Commonly, the deployed optical network involves the use of a standard integrated equipment as photodiodes, which do not provide a system monitoring from a frequency content point of view. Having Raman amplification a broad-band impact, fixed pre-calculated emulative approaches are not efficient for optimizing the amplifiers' working point, especially in a scenario affected by external modifications and spectral load variations. On the other hand, the adoption of this kind of amplification systems is necessary for realizing or upgrading long-reach transmission optical transport networks (OTNs). Furthermore, the investment required to fill the whole network equipment infrastructural gap could be not feasible, and so amplification sites have to be handled by means of the available feedback instrumentation. Previously, the authors addressed Raman amplification automation focusing on the amplifier operative phase and considering optical channel monitors (OCMs) as feedback sensors [5], [6]. In this work, we define an embedded controller architecture to autonomously manage Raman amplification for a single fiber span given already installed standard integrated equipment only. In particular, the amplifier operation is optimized to achieve accurate performance in terms of gain and tilt on the base of the physical layer information extracted by a specific probing procedure to characterize the fiber span, using EDFA integrated photodiodes. The proposal has been set up in laboratory and validated through a consistent experimental session, testing at first the probing procedure on a single fiber span and then the operation of a Raman amplifier using the extracted information.

## II. CONTROLLER ARCHITECTURE

Let introduce the conceived embedded controller architecture for Raman amplification, contextualizing its behavior within an optical network (Fig. 1). We assume that the transmission operative phase starts with the definition of the working point by the control plane, imparting the amplification constraints, a mean gain target, $\overline{G_{\mathrm{OO,tar}}}$, and a tilt target, $m_{G_{\mathrm{OO}},\mathrm{tar}}$, to each Raman amplifier along a specific optical link. Raman cards have an on-board software constituted by two units: the Raman Design Unit (RDU) and the Raman Control Unit (RCU) [5]. The RDU designs the Raman pumps power configuration that matches the targets by evaluating the optimal working point exploiting a numerical solver [7] on the base of the physical layer information extracted during an hypothetical probing phase. Then, the RCU sets Raman pumps and tracks the mean gain performing an analytical linearization around the optimal working point that relies on the evaluation of power gradients with respect to the gain variation. The control of Raman pumps is operated in order to maximize the match between the mean and the target gains thanks to the feedback received by the integrated photodiodes. This behavior confers a high degree of adaptability to the system in case of scenario modifications (e.g. component aging) or spectral load variations. Before starting with the operative phase, the system undergoes a well-defined probing procedure to properly characterize the physical layer. This method allows to probe all the fiber spans along a single optical line in series loading an ASE noise spectrum generated by the booster and measuring by means of the integrated photodiodes. The use of an ASE noise spectrum during the probing phase provides a significant advantage from a practical point of view because it allows to perform all the span measurements independently from the definition of a certain channel spectrum. At the end of the probing procedure, we assume that the RDU pre-calculates a look-up-table containing a Raman pump power configuration for all the on-off gain target values that the control plane can require. During the operative phase, only the RCU operates in order to counteract possible on-off gain variations. In this scenario, the proposed architecture would also serve to be an effective, real-time solution that enables an edge computing framework to be implemented.
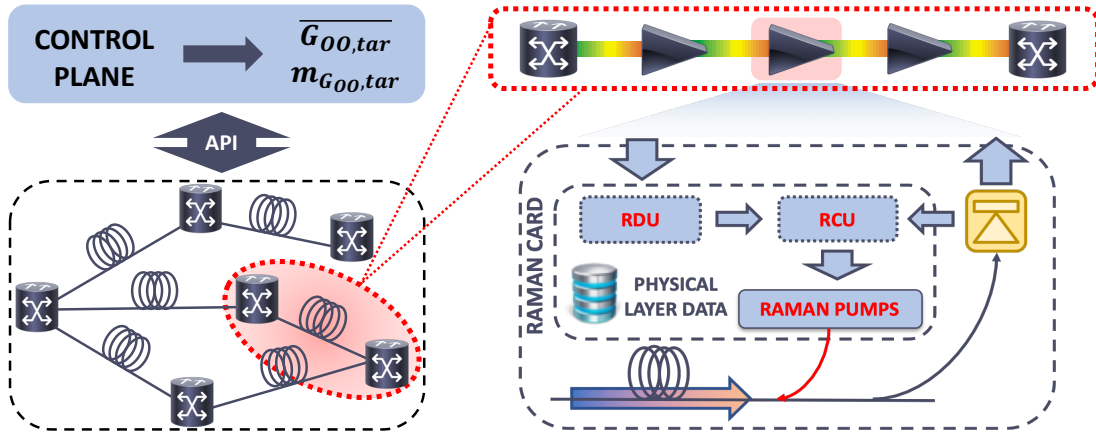
Fig. 1. Conceived embedded controller architecture for Raman amplification in a context of disaggregated optical transport network.

## III. EXPERIMENTAL SETUP

The general scheme of the equipment used to realize the proposed measurements is shown in Fig. 2. It is composed by a standard single mode fiber (SSMF) span with 85 km nominal length (created joining two SSMF spools of 60 km and 25 km nominal lengths) and two optical nodes: the transmitter node and the optical line amplifier node. The former is composed by a system of 35 polarized, continuous-wave (CW) distributed feedback (DFB) lasers, 100 GHz spaced, used to generate the C-band WDM spectrum. By using a CW comb we do not lose in generality, as Raman gain is not sensitive to the signal modulation but only to the average power level. The power level of each DFB laser is tuned to obtain an almost flat spectrum around 0 dBm per channel, after the EDFA amplification. The latter node is composed by a set of 4 counter-propagating Raman pumps with frequencies roughly at 204, 206, 209 and 211 THz, followed by an EDFA stage for WDM comb propagation through the rest of the link (out of the scope of this work). An optical spectrum analyzer (OSA) is used at both fiber span terminals in order to check the effectiveness of the probing phase only.

## IV. PROBING PROCEDURE

The presented probing procedure supports C-band transmission operations aiming to extract the loss coefficient function

for pump and channel frequencies, $\alpha(f_p)$ and $\alpha(f_{ch})$, the Raman efficiency, $C_R(\Delta f)$, and an additional gain correction parameter, $\overline{G_{OO,cor}}$, which is a Raman amplifier tuning parameter.

We assume the following Raman efficiency expression:

$$C_R(\Delta f) = K_R \, c_R(\Delta f) \,, \tag{1}$$

where $c_R(\Delta f)$ is the normalized Raman efficiency profile dependent on the frequency distance between the specific couple of signals and $K_R$ is the scaling factor, or the Raman coupling intensity. Given the significant similarity between different fiber type characterizations [1], in this probing procedure we extract only the scaling factor, fixing the profile shape [8].

Firstly, each Raman pump is switched on individually (without input spectral load) and, by exploiting the integrated back-reflection photodiode ($PD_2$), attenuation coefficients at each Raman pump frequency are derived using the following formula [9]:

$$\alpha(f_p) \approx \frac{\kappa P(f_p, L_S)}{2 P_R(f_p, L_S)} \tag{2}$$

where $\kappa = 0.5 \times 10^{-7}$ m$^{-1}$ is the assumed Rayleigh back-scattering coefficient, $L_S$ is fiber span length, $P(f_p, L_S)$ is the Raman pump launch power level and $P_R(f_p, L_S)$ is the measured reflected power. The back-reflection photodiode $PD_2$ is present within the Raman amplification system for safety
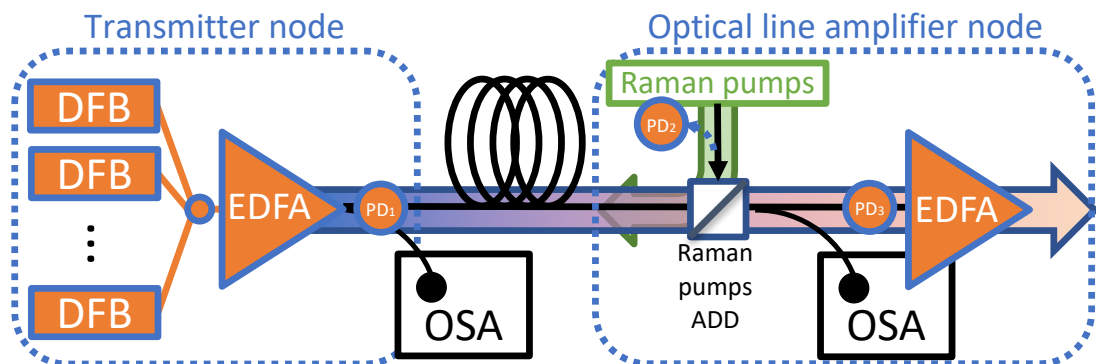


Fig. 2. Experimental equipment of a single optical fiber span at LINKS Foundation photonic laboratory, Turin.

reasons in order to detect fiber cut events and so to avoid power wasting. Even if the proposed approach requires to assume the value of the Rayleigh back-scattering coefficient $\kappa$, it allows to estimate the loss coefficients at the Raman pump frequencies without the need of an additional photodiode at the transmission node output able to measure the Raman pump residual power.

Secondly, the input spectrum is introduced loading ASE noise at low power level from the EDFA and, switching on one pump per time, the corresponding mean on-off gain $G_{OO}(f_{CH})$ is evaluated at C-band frequency range by measuring the received total power (PD$_3$). Knowing that the peak of the Raman efficiency curve is roughly at $\Delta f^{\mathrm{peak}} \approx 13.2\,\mathrm{THz}$, $f_{CH}$ represents the frequency around the C-band range that maximizes the coupling for the selected Raman pump

$$f_{CH} = f_p - \Delta f^{\mathrm{peak}}. \tag{3}$$

Being the system in undepleted pump condition, one value of Raman coupling is estimated for each on-off gain [10] and the related Raman scaling factor, $K_R$, is computed as follows:

$$K_R(f_p) = \frac{\ln(G_{OO}(f_{CH}))}{\mathcal{C}_R(f_p, f_{ch}^+, f_{ch}^-)P(f_p, L_S)L_{eff}(f_p)}, \tag{4}$$

where $P(f_p, L_S)$ is the launch power of the selected Raman pump in linear units, $\mathcal{C}_R(f_p, f_{ch}^+, f_{ch}^-)$ and $L_{eff}(f_p)$ are defined as:

$$\mathcal{C}_R(f_p, f_{ch}^+, f_{ch}^-) = \frac{\int_{f_p - f_{ch}^+}^{f_p - f_{ch}^-} c_R(\phi)\,d\phi}{f_{ch}^+ - f_{ch}^-}, \tag{5}$$

$$L_{eff}(f_p) = \frac{1 - e^{-\alpha(f_p)L_S}}{\alpha(f_p)}, \tag{6}$$

given $f_{ch}^+$, $f_{ch}^-$ the maximum and the minimum frequency of the input spectrum, respectively. The final Raman efficiency scaling factor, $\overline{K_R}$, is obtained as the average of the collected $K_R$ values.
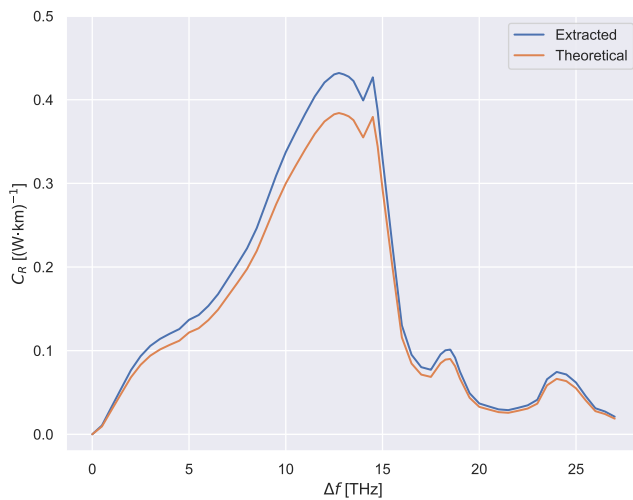
Subsequently, the average fiber attenuation at the C-band frequencies, $\overline{\alpha}$, is estimated as the difference of the total powers measured by the photodiodes PD$_1$ and PD$_3$ with all Raman pumps switched off.

To extract channel loss coefficients $\alpha(f_{ch})$, the expected mean on-off gains for each pump are computed, assuming the scaled profile found in the previous step as the effective Raman efficiency of the fiber span, $\overline{K_R}$, in order to probe the contribution of the fiber attenuation at channel frequencies. Consequently, the differences between the computed values and the measured ones $\Delta G_{OO}(f_{CH})$ are done and mapped on the loss coefficient function as:

$$\alpha(f_{CH}) = \overline{\alpha}\left(1 - \frac{\Delta G_{OO}(f_{CH})}{G_{OO}(f_{CH})}\right). \tag{7}$$

A quadratic regression is performed to determine the loss coefficient for each corresponding channel and to refine the complete function.

Finally, a first Raman amplification optimization is performed at the maximum gain target achievable by the system on the ASE spectrum as described in Sect. II. After this optimization, the actual mean on-off gain is extracted and compared with target value, computing the correction parameter as:

$$\overline{G_{OO,cor}} = \overline{G_{tar,MAX}} - \overline{G_{meas}}. \tag{8}$$

This final probing step aims to compensate for any uncertainty due to the lack of physical layer knowledge, improving the definition of the RDU operation and allowing a feasible procedure with an high degree of linearization for the RCU. During the operative phase of the system, all the variations of the working point due to input spectral load modifications are managed by the RCU.

## V. RESULTS

Executing the described probing procedure on the experimental setup, the extracted Raman efficiency (Fig. 3) is similar to the theoretical one associated to SSMF and even the estimated loss coefficient function trend (Fig. 4) is reasonable



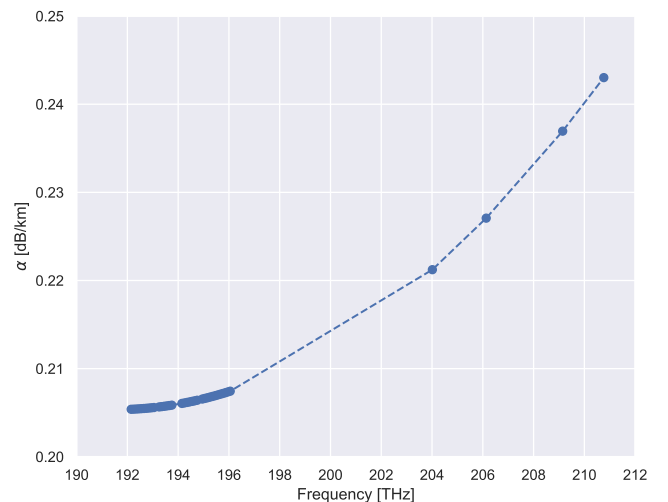Fig. 3. Probing outcome: Raman efficiency.



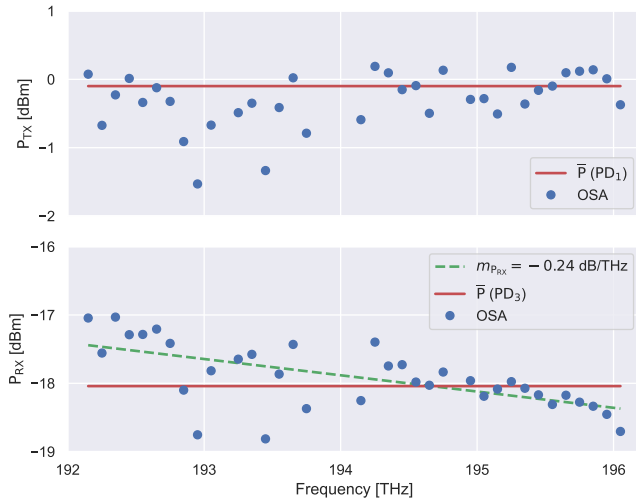Fig. 4. Probing outcome: loss coefficient function.

Fig. 5. Transmitted and received spectrum power profiles measured by OSA and photodiodes with Raman pumps turned off, where $m_{\mathrm{P_{RX}}}$ is the received spectrum profile tilt.

TABLE I
RAMAN PUMP POWER CONFIGURATION.

| $\overline{G}_{\mathrm{OO,tar}}$ [dB] | $P_{P,1}$ [mW] | $P_{P,2}$ [mW] | $P_{P,3}$ [mW] | $P_{P,4}$ [mW] |
|---|---|---|---|---|
| 13 | 261.6 | 124.8 | 244.2 | 93.6 |

with respect to literature [11], deducing an average link loss of about 18 dB.

Starting from the physical layer information extracted during the probing procedure, the embedded controller architecture has been tested imparting as amplification constraints a mean gain target of 13 dB, due to the maximum Raman pump power limits, and a flat WDM spectrum at the optical line amplifier node. This goal results to be extremely challenging for the apparatus under analysis due to the required high performance and the impossibility to detect any information about the system frequency behavior in standard operations. The measurements of the transmitted and received power spectra are reported in Fig. 5. The final Raman pump power level configuration deployed by the controller is reported in Tab. I, with Raman pumps ordered for decreasing frequencies. The received power spectrum and the on-off gain profile are shown in Fig. 6. Considering the linear regression of the WDM spectrum, the residual tilt captured by the OSA is less than 1 dB over the total C-band and the mean gain target has been accurately achieved.

## VI. CONCLUSION

In this work, we proposed and tested an embedded controller architecture for single fiber span that, harmonized with the ad-hoc conceived probing procedure, allows to handle Raman amplification using standard integrated network equipment. In particular, the initial probing phase provides the information needed by the controller in order to perform an autonomous and flexible management.
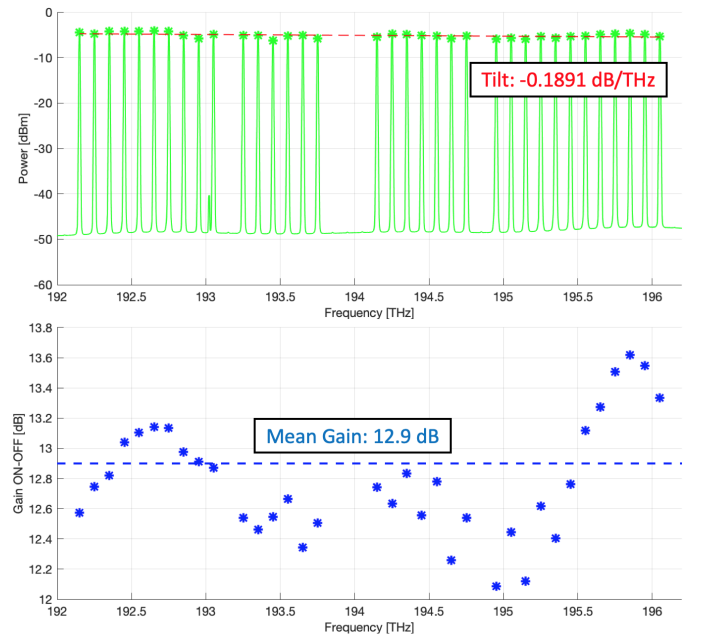


Fig. 6. Experimental results: received power spectrum and on-off gain profile.

## REFERENCES

[1] J. Bromage, "Raman amplification for fiber communications systems," *Journal of Lightwave Technology*, vol. 22, no. 2, p. 79, 2004.
[2] M. N. Islam, "Raman amplifiers for telecommunications," *IEEE journal of selected topics in quantum electronics*, vol. 8, no. 3, pp. 548–559, 2002.
[3] A. Ferrari, M. Cantono, U. Waheed, A. Ahmad, and V. Curri, "Networking benefits of advanced dsp techniques and hybrid fiber amplification," in *2017 19th International Conference on Transparent Optical Networks (ICTON)*. IEEE, 2017, pp. 1–4.
[4] V. Curri and A. Carena, "Merit of raman pumping in uniform and uncompensated links supporting nywdm transmission," *Journal of Lightwave Technology*, vol. 34, no. 2, pp. 554–565, 2015.
[5] G. Borraccini, A. Ferrari, S. Straullu, A. Nespola, A. D'Amico, S. Piciaccia, G. Galimberti, A. Tanzi, S. Turolla, and V. Curri, "Softwarized and autonomous raman amplifiers in multi-band open optical networks," in *2020 International Conference on Optical Network Design and Modeling (ONDM)*. IEEE, 2020, pp. 1–6.
[6] G. Borraccini, S. Straullu, A. Ferrari, S. Piciaccia, G. Galimberti, and V. Curri, "Flexible and autonomous multi-band raman amplifiers," in *2020 IEEE Photonics Conference (IPC)*, 2020, pp. 1–2.
[7] A. Ferrari, M. Filer, K. Balasubramanian, Y. Yin, E. Le Rouzic, J. Kundrát, G. Grammel, G. Galimberti, and V. Curri, "Gnpy: an open source application for physical layer aware open optical networks," *Journal of Optical Communications and Networking*, vol. 12, no. 6, pp. C31–C40, 2020.
[8] J. Bromage, K. Rottwitt, and M. Lines, "A method to predict the raman gain spectra of germanosilicate fibers with arbitrary index profiles," *IEEE Photonics Technology Letters*, vol. 14, no. 1, pp. 24–26, 2002.
[9] P. Hansen, L. Eskildsen, J. Stentz, T. Strasser, J. Judkins, J. DeMarco, R. Pedrazzani, and D. DiGiovanni, "Rayleigh scattering limitations in distributed raman pre-amplifiers," *IEEE Photonics Technology Letters*, vol. 10, no. 1, pp. 159–161, 1998.
[10] E. Pincemin, D. Grot, L. Bathany, S. Gosselin, M. Joindot, S. Bordais, Y. Jaouen, and J.-M. Delavaux, "Raman gain efficiencies of modern terrestrial transmission fibers in s-, c-and l-band," in *Nonlinear Guided Waves and Their Applications*. Optical Society of America, 2002, p. NLTuC2.
[11] S. Walker, "Rapid modeling and estimation of total spectral loss in optical fibers," *Journal of lightwave technology*, vol. 4, no. 8, pp. 1125–1131, 1986.